Journal of Power Sources 192 (2009) 562–572

Contents lists available at ScienceDirect

Journal of Power Sources

journal homepage: www.elsevier.com/locate/jpowsour

# Feasibility investigations on multi-cutter milling process: A novel fabrication method for microreactors with multiple microchannels

Minqiang Pan[a,*], Dehuai Zeng[a,b], Yong Tang[a]

[a] School of Mechanical and Automotive Engineering, South China University of Technology, Guangzhou 510640, China
[b] School of Mechatronics and Control Engineering, Shenzhen University, Shenzhen 518060, China

ARTICLE INFO

*Article history:*
Received 11 February 2009
Received in revised form 10 March 2009
Accepted 11 March 2009
Available online 24 March 2009

*Keywords:*
Multi-cutter milling
Slotting cutter
Microchannel reactor
Laminated sheet

ABSTRACT

A novel multi-cutter milling process for multiple parallel microchannels with manifolds is proposed to address the challenge of mass manufacture as required for cost-effective commercial applications. Several slotting cutters are stacked together to form a composite tool for machining microchannels simultaneously. The feasibility of this new fabrication process is experimentally investigated under different machining conditions and reaction characteristics of methanol steam reforming for hydrogen production. The influences of cutting parameters and the composite tool on the microchannel qualities and burr formation are analyzed. Experimental results indicate that larger cutting speed, smaller feed rate and cutting depth are in favor of obtaining relatively good microchannel qualities and small burrs. Of all the cutting parameters considered in these experiments, 94.2 m $min^{-1}$ cutting speed, 23.5 mm $min^{-1}$ feed rate and 0.5 mm cutting depth are found to be the optimum value. According to the comparisons of experimental results of multi-cutter milling process and estimated one of other alternative methods, it is found that multi-cutter milling process shows much shorter machining time and higher work removal rate than that of other alternative methods. Reaction characteristics of methanol steam reforming in microchannels also indicate that multi-cutter milling process is probably suitable for a commercial application.



## 1. Introduction

Microchannel reactors present several advantages for performing chemical reaction compared with traditional technologies. The microchannels with maximum characteristic dimension of 500 μm provide high surface-to-volume ratios as well as rapid heat exchange and mass transfer rates, hence drastically reduced volumes and improved process efficiency can be expected.

The methods of incorporating microchannels into reactors can be classified into two categories, as shown in Fig. 1, a single microchannel is generally fabricated on the surface of a solid to form a monolithic construction to serve a single reaction [1–4], whereas multiple sheets patterned with parallel microchannels are stacked and then bonded together to yield a laminated-sheet component [5–7]. As laminated-sheet structure enables the integration of multiple unit operations, including flow distribution, heat exchange, mixing, chemical reaction, or chemical separation in the same component [8], it is regarded as one of the preferred constructions for microchannel reactors.

Fig. 2 presents the two fundamental different constructions of plates containing parallel microchannels. One is the plate with parallel microchannels only [9–10], the other is microchannels with manifold structures [11–14]. Although it is economical and highly efficient to machining the first kind of plate structure by wire cutting technology, it needs additional flow distribution regions. Since the manifold can effectively enhance flow uniformity among microchannels to improve the reaction performances, the second construction has been gradually applied in multiple fields.

The machining efficiency and manufacturing cost have become the primary barriers for the commercial production of microchannel reactors. Various fabrication techniques have been applied to construct microchannels with manifolds, including LIGA (Lithographie Galvanoformung Abformung) process [1], wet or dry etching process [12–14], electrodischarge machining (EDM) [15], ion etching [16], micro-turning and milling technology [17,18], each with their specific application ranges and relative merits. However, the option of fabrication techniques should take cost and efficiency into account to avoid developing a laboratory curiosity rather than a commercially feasible method. Although these techniques provide unique advantages in the fabrication of three-dimensional structures, they are either quite time-consuming or costly. Furthermore, these techniques are particularly well suited for fabricating microstructures ranging from hundreds to thousands of microns. Their superiorities would not be given full play to fabricate multiple parallel microchannels with manifolds on a large area sheet. Therefore, an economical micro-fabrication technology should be

* Corresponding author. Tel.: +86 20 8711 4634; fax: +86 20 8711 4634.
*E-mail address:* mqpan@scut.edu.cn (M. Pan).

0378-7753/$ – see front matter © 2009 Elsevier B.V. All rights reserved.
doi:10.1016/j.jpowsour.2009.03.024

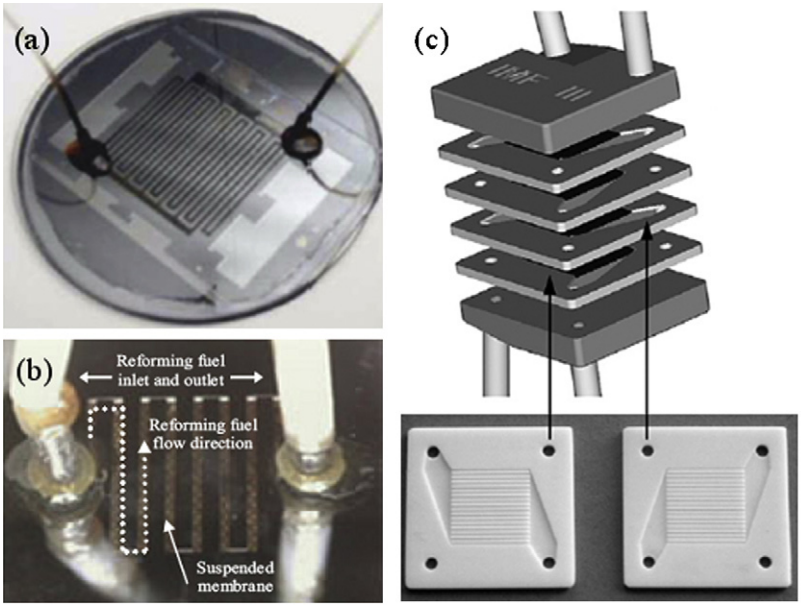


**Fig. 1.** Two methods of incorporation microchannels into reactors. (a) and (b) monolithic construction with a single microchannel [1–3]. (c) Laminated-sheet construction with parallel microchannels [5].

developed to fabricate multiple parallel microchannels with manifolds. In this work, a novel multi-cutter milling process for multiple parallel microchannels with manifolds is proposed to address the challenge of mass manufacture as required for cost-effective commercial applications. section2. Description of multi-cutter milling process

### 2.1. Fabrication principle

Rarefaction effects occur adjacent to the walls when the characteristic dimensions of microchannels become comparable to the molecular mean free path of the process fluid, which is characterized by the Knudsen number, *Kn*, defined as the ratio of the molecular mean free path to the characteristic length. For small Knudsen numbers, $Kn \leq 10^{-3}$, the fluid is considered to be a continuum and Navier–Stokes equations are applicable, whereas for large values, $Kn \geq 10$, non-continuum regions appear in the fluid, which affects the velocity profile, pressure drop and heat transfer in the channels [19]. Since relatively large characteristic dimensions of microchannels applied in the microchannel reactors are favorable to avoid the emergence of rarefaction effects and reduce the manufacturing cost, the microchannel widths in a majority of developed microchannel reactors are designed in the range of 200–500 μm, as described in Table 1.

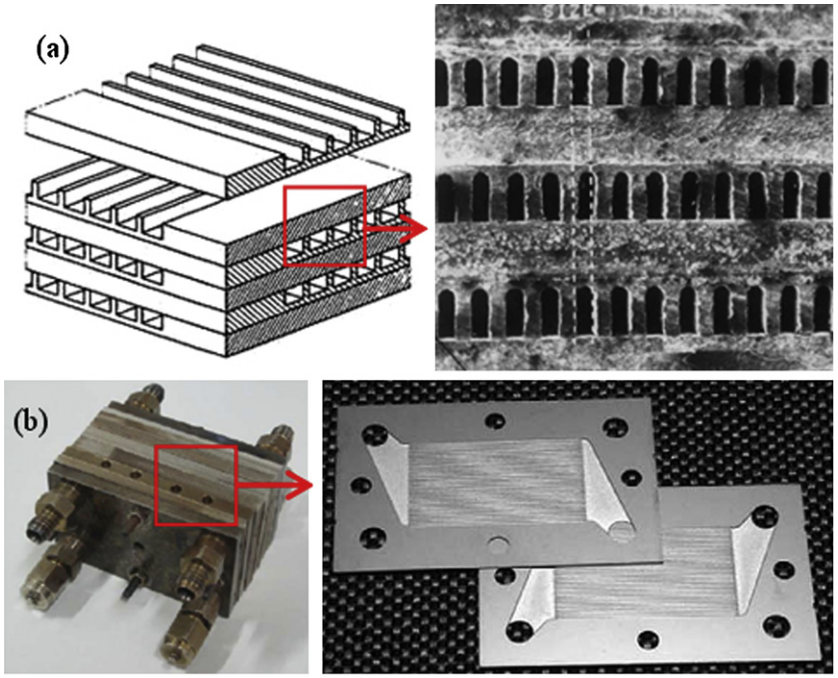


**Fig. 2.** Two fundamental different constructions of plates. (a) Principle sketch of a cross-flow micro heat exchange and the SEM photo of the microchannels [9]. (b) Laminated plates construction containing microchannels with manifold [11–12].

**Table 1**
The microchannel structural parameters in the developed microchannel reactors.

| Researchers | Structure parameters of microchannels (length × width × depth) | Microchannel number | Application field |
|---|---|---|---|
| Park et al. [12] | 34 mm × 300 μm × 200 μm | 34 | Integrated microchannel methanol processor |
| Chen et al. [13] | 30 mm × 500 μm × 170 μm | 48 | CO selective oxidation microchannel reactor |
| Delsman et al. [14] | 40 mm × 400 μm × 300 μm | 29 | CO preferential oxidation microdevice |
| Ryi et al. [20] | 17 mm × ø500 μm × 250 μm | 22 | Methane steam reformer |
| Park et al. [21] | 33 mm × 500 μm × 200 μm | 20 | Microchannel methanol steam reformer |
| Sohn et al. [22] | 100 mm×450 μm × 150 μm | 12 | Integrated menthanol fuel processor |
| Cominos et al. [23] | 30 nm × 250 μm × 187 μm | 82 | CO preferential oxidation reactor |
| Tonkovich et al. [24] | 35 mm × 254 μm × 1500 μm | 37 | Methane partial oxidation reactor |

Since microchannel widths are usually chosen to be between 200–500 μm, the slotting cutter, the thickness of which is in the range of 100–500 μm and minimum diameter is larger than 20 mm, opens possibilities for fabricating microchannels, especial for high-aspect-ratio microchannels. The slotting cutter is generally applied for splitting the materials by a narrow slit. As shown in Fig. 3, the cutter has several blades, and the rake and back angles are in the range of 3–5° and 11–16°, respectively. As described in Table 1, since the practical microchannel number on a plate is adequately large, several slotting cutters are stacked together to form a composite tool for simultaneously machining microchannels in this work. As presented in Fig. 3, the composite tool consists of a handle, a lock gasket, a locknut, five slotting cutters and four gaskets. The slotting cutters and gaskets are alternately stacked together and fixed by the lock gasket and locknut for easy replacement. The composite tool is assembled inside the spindle by the handle.

Fig. 4 presents two methods to fabricate parallel microchannels by the composite tool, one is end milling, and the other is horizontal milling. During the fabrication process, the two manifolds in the plate are firstly fabricated by another milling tool, and then the plate with two manifolds is arranged vertical to the tool and located on a mounted plate by four fixed bolts, while the mounted plate is fixed by a vice. The fabrication of the length and depth of the microchannel is achieved by the combination of primary rotary of composite tool as well as the movement of worktable in *x* and *y* direction, respectively, whereas the fabrication of the width is combined by the tool rotary and movement in *z* direction.

### 2.2. Burr formation

Unlike conventional micro-machining methods, which utilize miniature milling, drilling and turning tools as small as 10 μm in diameter to produce micro-scale features [25], the multi-cutter milling process uses conventional large-scale cutter to machining microchannels. Therefore, the mechanics of multi-cutter milling process significantly differs from conventional micro-machining methods due to the rescaling of the tool dimension, the change in the tool geometry and machining conditions.

The differences between the tools arise from the ratio of cutting edge radius to the chip thickness, as depicted in Fig. 5. In the conventional micro-machining methods, the cutting edge radius is approximately closed to or even larger than the chip thickness. The entire material is forced under the tool due to large effective rake angles and then deformed. The elastic deformation recovers after the tool passes. Some of the forced material is removed and others form relatively large burrs with respect to the uncut chip thickness. In addition, the relatively small chip thickness due to small cutting edge radius results to low machining efficiency, especially for the fabrication of high-aspect-ratio microchannels.

As shown in Fig. 5(b), the cutting edge radius is much smaller than the chip thickness in the multi-cutter milling process. The chip

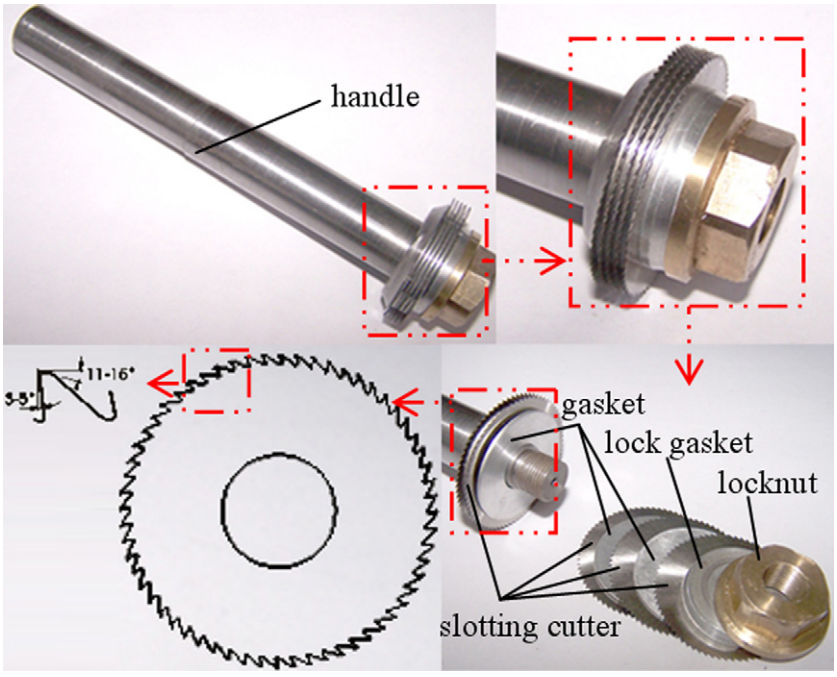


**Fig. 3.** The composite tool stacked by multiple slotting cutters.

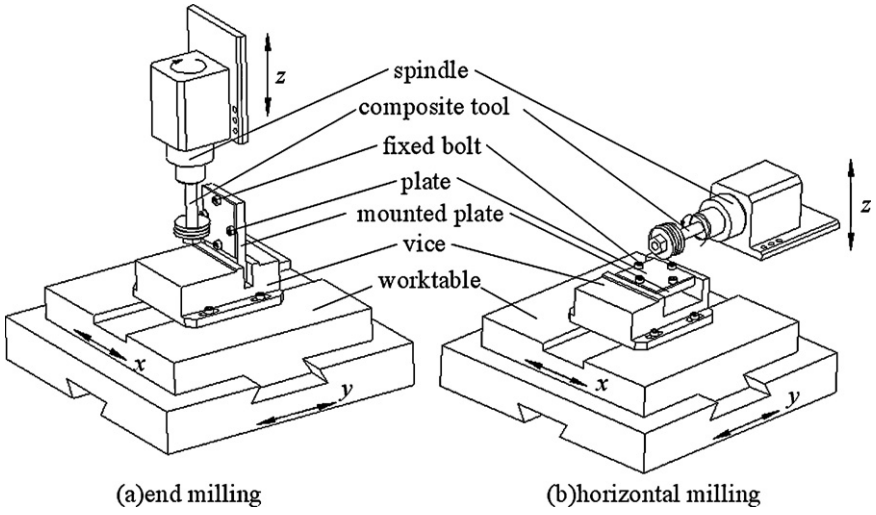


**Fig. 4.** Fabrication principle of multi-cutter milling process.

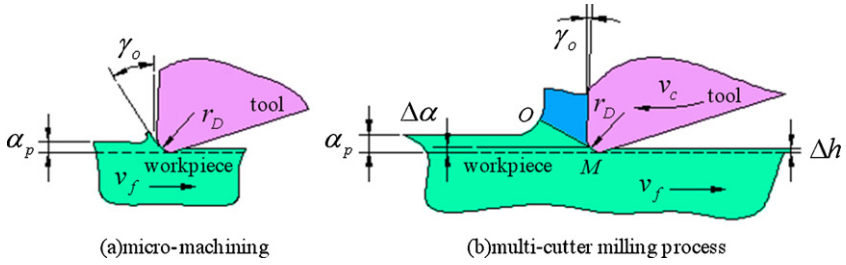


**Fig. 5.** The principle of burr formation.

formation is similar to the one in conventional large-scale cutting process. The cutting lay is forced and shear deformed under the action of cutting edge, and then formed into chip and slip along the shear plane OM. However, a cutting lay with thickness of $\Delta\alpha$ could not slip along the shear plane due to the cutting edge radius. The cutting lay causes plastic deformation and then flows outside along the tool flank under the coactions of ploughing and friction. After the tool passes, elastic deformation recovers and this cutting lay resumes a height of $\Delta h(\Delta h < \Delta\alpha)$, then this recovery lay flows out the top sides of microchannels and forms into burrs at the top edges.

Although the mechanics of multi-cutter milling process is similar to that of conventional large-scale cutting process, burrs are relatively large and hard to remove when the multi-cutter milling process is used to machining microchannels. In the following section, the feasibility of new fabrication process is experimentally investigated under different machining conditions and the influences of cutting parameters and the composite tool on the microchannel qualities and burr formation are analyzed.

## 3. Experimental setup and methodology

### 3.1. Machining of microchannels

The experiments were undertaken on a conventional end milling machine, as shown in Fig. 6. The slotting cutter used was a high speed steel tool and measured ø40 mm in diameter. The cutter had 72 tool edges and each with 5° rake angle and 15° back angle. The tool gasket measured ø35 mm in the diameter. Red copper was chosen as the work material.

During experiments, only one cutter was firstly used to fabricate microchannels for the investigation of the influences of machining parameters on the burr formation. Five cutting speeds (7.5, 14.8, 29.5, 59.7 and 94.2 m $min^{-1}$), five feed rates (23.5, 30, 47.5, 60 and 75 mm $min^{-1}$) and two cutting depths (0.5 and 1 mm) were considered in the experiments.

Then a composite tool assembled by five cutters was applied for the fabrication to analyze the influences of tool parameters on microchannel qualities and burr formation. Three different cutter thicknesses (0.2, 0.3 and 0.4 mm) were investigated.

Next, a plate with dimension of $85 \times 85 \times 2$ $mm^3$ used for a laminated reactor was selected to estimate the potentials of multi-cutter

**Fig. 6.** On site machining.

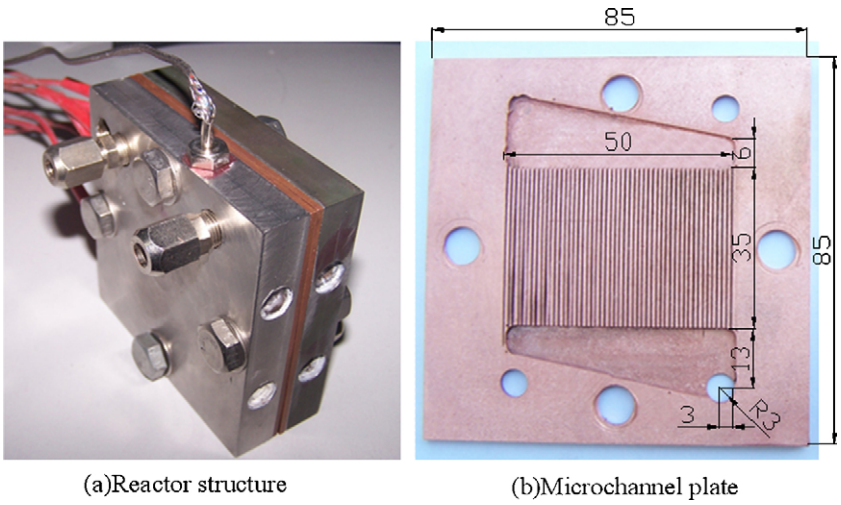


**Fig. 7.** Microchannel plate structure.

milling process for practical use, and the machining efficiency was compared with other micro-machining methods. As shown in Fig. 7, each plate had 50 parallel microchannels with dimensions of 270 μm in width, 1000 μm in depth and 35 mm in length. Other structural parameters were shown in Fig. 7(b). The fabrication of microchannel plate included two steps, one was the machining of microchannels, and the other was the machining of two manifolds and other holes. Here only the former was selected to analyze the differences of machining time and work removal rate between multi-cutter milling process and other alternative methods on the basis of other research findings. Here work removal rate was defined by dividing the work removal volume with machining time [26].

### 3.2. Burr measurement

In the multi-cutter milling process, the slotting cutter is firstly cut in the workpeieces from the bottom, and finally cut out from the top side of microchannel, which forms three kinds of burrs, they are entrance, exit and top burrs [27,28], as shown in Fig. 8. Top and exit burrs for different machining conditions were investigated in this study since they was relatively large and difficult to remove.

SEM images of burrs were collected to qualitatively analyze the influences of machining conditions and tool parameters on the burr formation. The top burrs were usually of large and wavy type [25,29]. It was found in the experiments that top burrs on the both sides of microchannels were irregular shapes, an estimated method for calculating the width values of top burrs was applied here.

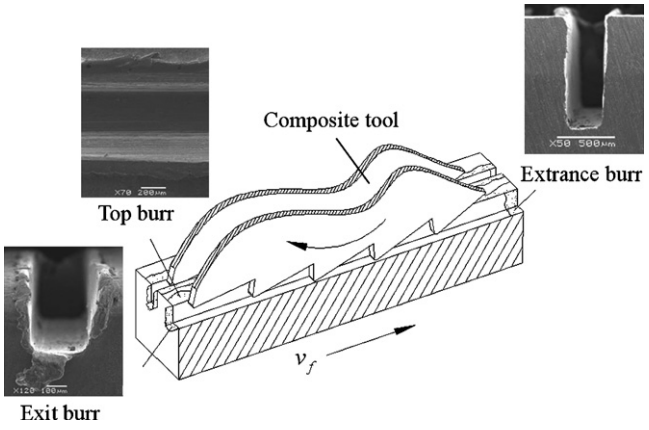


**Fig. 8.** Three kinds of burrs formed by multi-cutter milling.

The widths of wave crests in a certain length $L$ are measured and averaged as the unilateral width of top burrs, as shown in Fig. 9. The width of top burrs is defined as the average of unilateral widths in both sides.

$$W = \frac{1}{2}\left(\frac{1}{N_i}\sum_{i=1}^{N_i} W_i + \frac{1}{N_j}\sum_{j=1}^{N_j} W_j\right) \quad (1)$$

where $N_i$ and $N_j$ represent the number of the wave crest in both sides. $W_i$ and $W_j$ are the crest width of the top burrs in both sides, respectively. Fig. 10

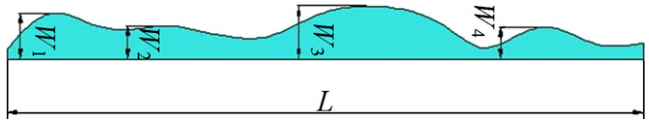


**Fig. 9.** The calculation of unilateral width of top burrs.

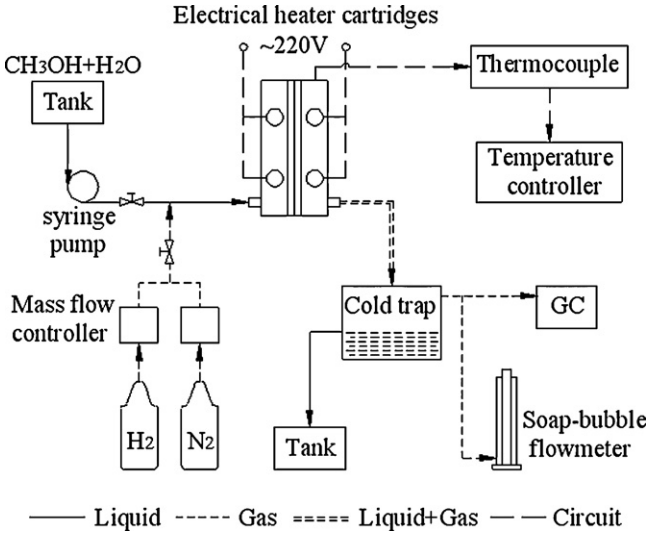


**Fig. 10.** Schematic illustration of experimental setup for reaction.

### 3.3. Reaction for methanol steam reforming

Aiming at practice application, the reaction characteristics of methanol steam reforming in the microreactor presented in Fig. 7 were experimental investigated in this work. Methanol steam reforming was selected because it would offer the highest attainable hydrogen concentration, of up to 75%, and a relative small amount of carbon monoxide [30,31].

Since methanol steam reforming was an endothermic reaction, two holes were drilled in each cover plate for loading electrical heater cartridges to supply the necessary heat, and a thermocouple was inserted to one of the cover plates to control the reaction temperature. In the stage of experiments, two microchannel plates were assembled inside the reformer, the first one used for evaporation and the other for reaction. The overall dimension of reformer excluding fittings was about $85 \times 85 \times 30\,mm^3$.

Firstly, a Cu/Zn/Al/Zr catalyst for methanol steam reforming was prepared by co-precipitation method as described previously [32], and then the catalyst was deposited inside the microchannels by washcoating method as following: The surfaces of microchannels was precoated by an alumina–sol as a barrier layer, then washcoated with an aqueous suspension of Cu/Zn/Al/Zr catalyst on the preformed alumina layer. The resulting precursor of catalyst-coated metal plate was calcined at 400–600 °C for 2 h under nitrogen atmosphere. The total amount of catalyst coated in the microchannels was 0.2 g.

Fig. 10 showed the schematic diagram of experimental setup for reaction. The catalyst was activated in a $H_2/N_2$ mixture flowing with a volume ratio of 1:4 at 300 °C for 2–3 h. After the catalyst activation, the mixture of methanol and water in 1:1.3 molar ratios was firstly gasified in the first plate and then supplied into the second plate for reforming by a syringe pump. The residual methanol and moisture were separated by a cold trap. While the steam reforming reaction was progressing steadily, the composition of reformate was analyzed by a gas chromatograph equipped with a TCD detector. The flow rate of reformate was measured by a soap-bubble flowmeter.

The preliminary experimental results showed that the hydrogen production rate was relatively low with low reaction temperatures due to the small amounts of catalysts in microchannels. Therefore, two relative high reaction temperatures were selected in the experiments, i.e. 400 °C and 450 °C, and the gas hourly space velocity (GHSV) were varied to investigate the reformer performances.

The methanol conversion, hydrogen selectivity and hydrogen production rate are defined as follows, respectively.

$$X_{MeOH} = \frac{F(y_{CO} + y_{CO_2})}{22.4 \times n_{MeOH,in}} \times 100\% \quad (2)$$

$$S_{H_2} = \frac{F(3C_{CO_2} + 2C_{CO})}{3 \times n_{MeOH,in}} \times 100\% \quad (3)$$

$$Y_{H_2} = X_{MeOH} \times S_{H_2} \quad (4)$$

where $F$ is the normal flow rate of effluent gas, $y$ is the volumetric fraction and $C$ is the concentration in the reformate. $n_{MeOH,in}$ is the molar flow rate of methanol fed into the microreactor.

## 4. Results and discussion

### 4.1. The influences of cutting parameters on burr formation

#### 4.1.1. Cutting speed and feed rate

The widths of top burrs were plotted in Fig. 11 as a function of cutting speed and feed rate. It could be clearly seen that the burr widths increased with the decreased cutting speed or increased feed rate. Larger chip formed as cutting speed decreased or feed rate increased, and the friction between the tool and chip increased, leading to a corresponding increase in the plastic strain associated with chip formation, and hence the burr widths increased.

On the condition of 30 mm $min^{-1}$ feed rate and 0.5 mm cutting depth, the maximum burr width reached to 149.6 μm when the cutting speed was 7.5 m $min^{-1}$, as shown in Fig. 11(a). For 29.5 m $min^{-1}$ cutting speed and 0.5 mm cutting depth, Fig. 11(b) indicated that the burr width reached the maximum value of 204.7 μm when the feed rate varied from 20 mm $min^{-1}$ to 70 mm $min^{-1}$. When the width of top burrs was larger than that of the interval between two microchannels, fash burrs were easily formed due to the overlapping top burrs of the adjacent microchannels, as shown in Fig. 12.

#### 4.1.2. Cutting depth

Fig. 13 presented how the widths of top burrs varied with the cutting depth on the condition of 29.5 m $min^{-1}$ cutting speed and 30 mm $min^{-1}$ feed rate. Obviously, the widths of top burrs increased with the increased cutting depth. It was because larger chip resulted in larger cutting force and plastic deformation, which gave rise to larger widths of top burrs.

For the same depth, the feed frequency in depth direction could show great influences on the widths of top burrs. As shown in Fig. 13, for the cutting depth of 1 mm, the width of top burr was 234.9 μm as feed once in depth direction, whereas the width value was 156.6 μm as feed twice, each for 0.5 mm in depth. Obviously, smaller width of top burrs was obtained by feeding twice in depth direction because each feeding could produce thin chips and the top burrs formed at the first cutting would be cracked by the second cutting and then overlapped by the top burrs produced by the second cutting.

When multiple cutters were stacked together, the rigidity of the tool became much worse. Excessive cutting depth would easily cause the cutters to be broken due to larger chip and excessive cutting force. Fig. 14 indicated that two cutters were torn up during fabrication when the cutting depth was 1.5 mm.

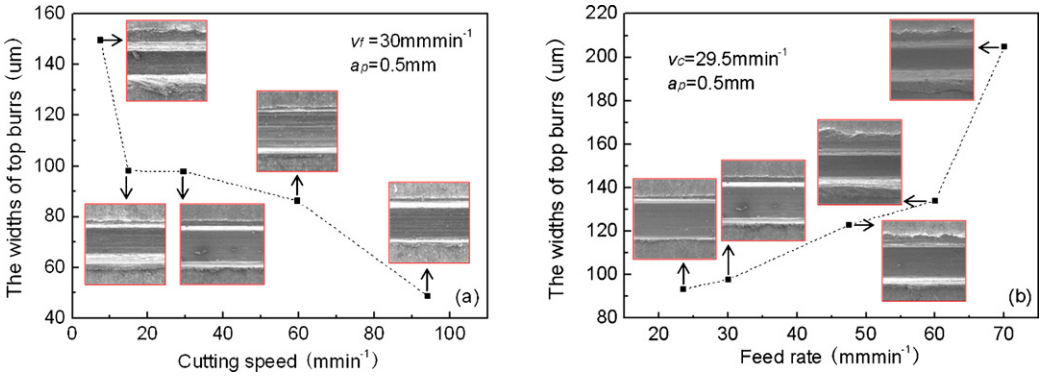


**Fig. 11.** Influences of cutting speed and feed rate on top burrs.

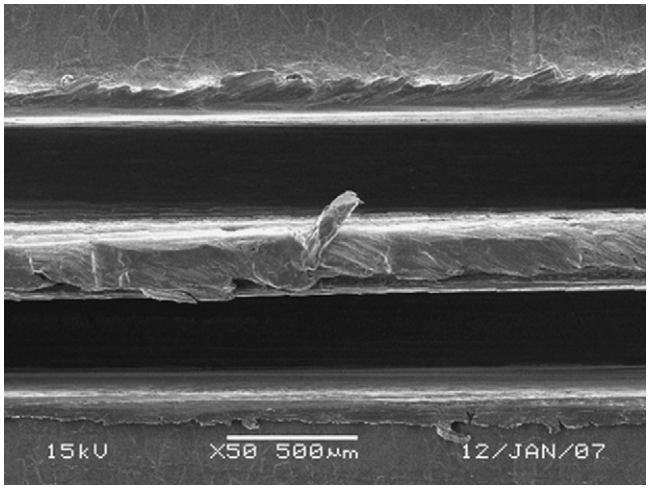


**Fig. 12.** Fash burr formation due to the overlapping top burrs.

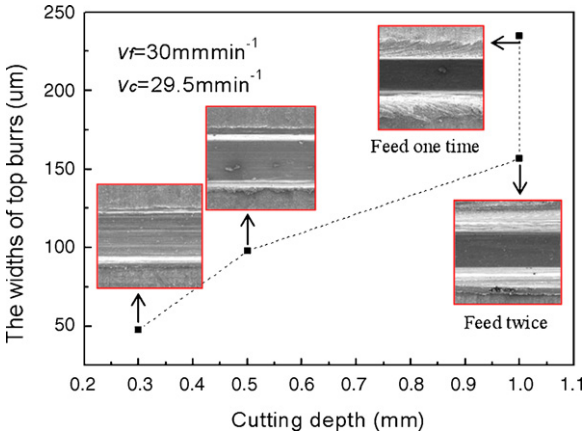


**Fig. 13.** Influences of cutting depth on the widths of top burrs.

The experimental results indicated that the exit burr formation was not strongly affected by the cutting speed and feed rate. However, the cutting depth showed great influences on the exit burrs, as shown in Fig. 15. The width of exit burr was approximately equal to the microchannel width. When the cutting depths were 1 mm and 0.25 mm, the corresponding height of exit burrs were 558 μm and 140 μm, respectively. The height of exit burr was almost linearly increased with the cutting depth.

### 4.2. The influences of composite tool on microchannel qualities and burr formation

#### 4.2.1. The number of stacked cutters

The composite tool was one of the important factors influencing the microchannels qualities and burr formation. Evidently, the maximum processing efficiency could be achieved when the stacked numbers of slotting cutters were equal to the microchannel numbers. However, stacking too many cutters together easily led to inconsistent concentricity among cutters, resulting in the inconsistent depth of microchannels, as shown in Fig. 16.

#### 4.2.2. Slotting cutter thickness

Figs. 17 and 18 indicated the influences of slotting cutter thickness on the top and exit burrs on the condition of 29.5 m $min^{-1}$ cutting speed, 30 mm $min^{-1}$ feed rate and 0.5 mm cutting depth. When the cutter thickness was changed from 0.2 μm to 0.4 μm, the width of top burrs increased from 98.3 μm to 128 μm. The width of exit burrs was almost the same as that of the microchannnel, but the height strongly increased with the cutter thickness. It could be concluded that the cutter thickness showed much influences on the formation of exit burrs rather than that of top burrs. Since most material removed from the middle of the channel while a small amount of chips flowed towards the top sides of microchannels, larger chip was produced when the cutter thickness became larger, which led to a corresponding increase in the height of exit burrs.

#### 4.2.3. The tool gasket

As depicted in Fig. 19, Eq. (5) defined the relations among the microchannel interval $W_s$, microchannel width $W_c$, slotting cutter thickness $E_t$ and gasket thickness $E_g$. In order to prevent the tool gaskets from touching the plate, the relation of the diameter of tool gaskets $D_g$ and cutter $D_t$ should satisfy the relation of Eq. (6).

$$E_g + E_t = W_s + W_c \tag{5}$$

$$\frac{1}{2}(D_t - D_g) > E \tag{6}$$

When $W_c$ and $E_t$ were determined, smaller $W_s$ would lead to smaller $E_g$, which would easily cause microchannels deformation due to the vibration appeared among multiple cutters, as shown in Fig. 20(a). Too small diameter of tool gasket also resulted to the vibration of cutters and introduced the cutters offset during the process, as presented in Fig. 20(b).

### 4.3. Comparison of other alternative methods

From the above experimental results, it could be found that relatively good microchannel qualities and small burrs were benefited from larger cutting speed, smaller feed rate and cutting depth. Of all the cutting parameters considered in the experi-

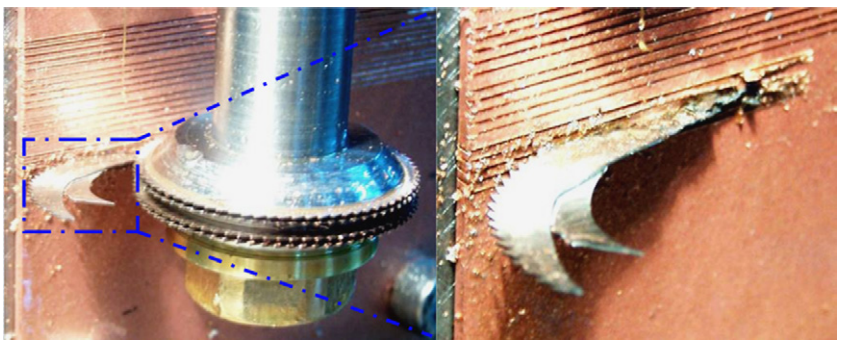

**Fig. 14.** Tool tore up due to excessive large cutting depth.

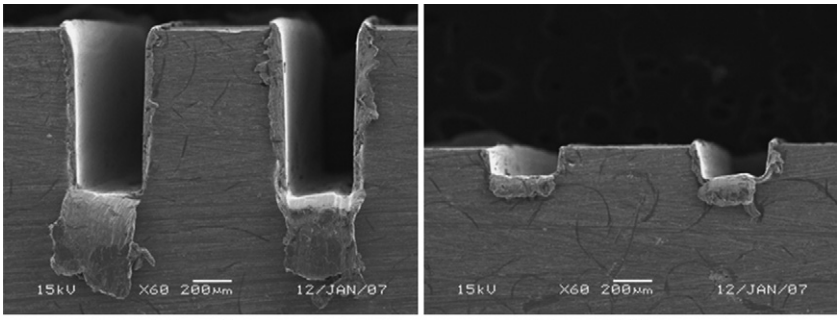


**Fig. 15.** The influence of cutting depth on the exit burrs.

ments, 94.2 m min$^{-1}$ cutting speed, 23.5 mm min$^{-1}$ feed rate and 0.5 mm cutting depth were found to be the optimum value. On this machining condition, the machining time and work removal rate of multi-cutter milling process were compared with that of three alternative methods, as shown in Fig. 21 . Here oil EDM milling, dry EDM milling and reactive ion etching were chosen due to their superiorities in the machining of microchannels. Fig. 21 also presented a comparison of the multi-cutter and single-cutter milling process.

The machining time and work removal rate of two EDM milling methods as well as reactive ion etching were estimated according the experimental results by Z. Yu et al. [26] and M. Kuhnke et al.

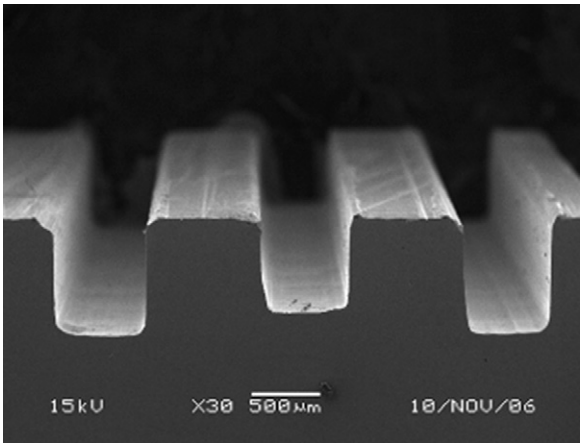


**Fig. 16.** The inconsistent depth of microchannels.

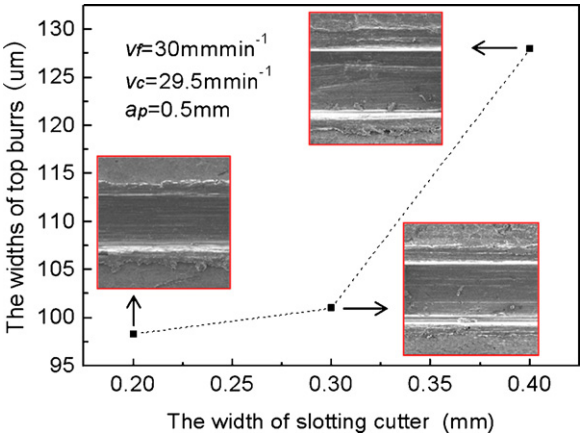


**Fig. 17.** Influence of slotting cutter thickness on the top burrs.

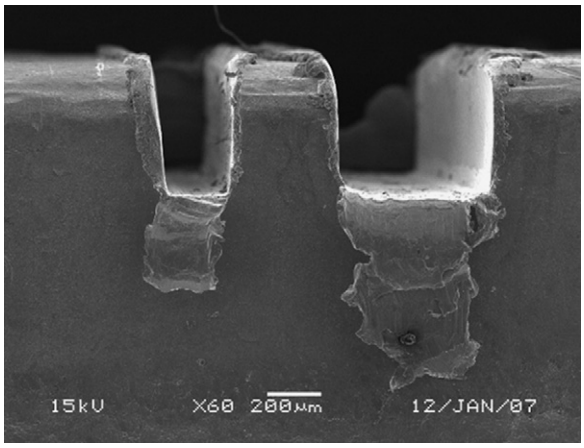


**Fig. 18.** Influence of slotting cutter thickness on the exit burrs.

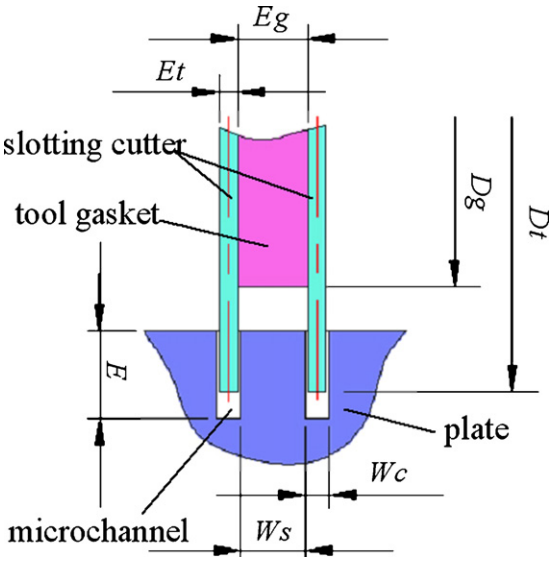


**Fig. 19.** Relationship among the microchannel, cutter and gasket.

[33], respectively. Although the estimated results might somewhat deviate from the experimental one due to the differences of the used work materials in the experiments, qualitative analysis would be provided on these machining methods.

According to the results, machining time of multi-cutter milling process was one-eighth and one-thirtieth lower than that of oil EDM milling and reactive ion etching, and work removal rate was eight and fifty times larger, respectively. The machining time of dry EDM

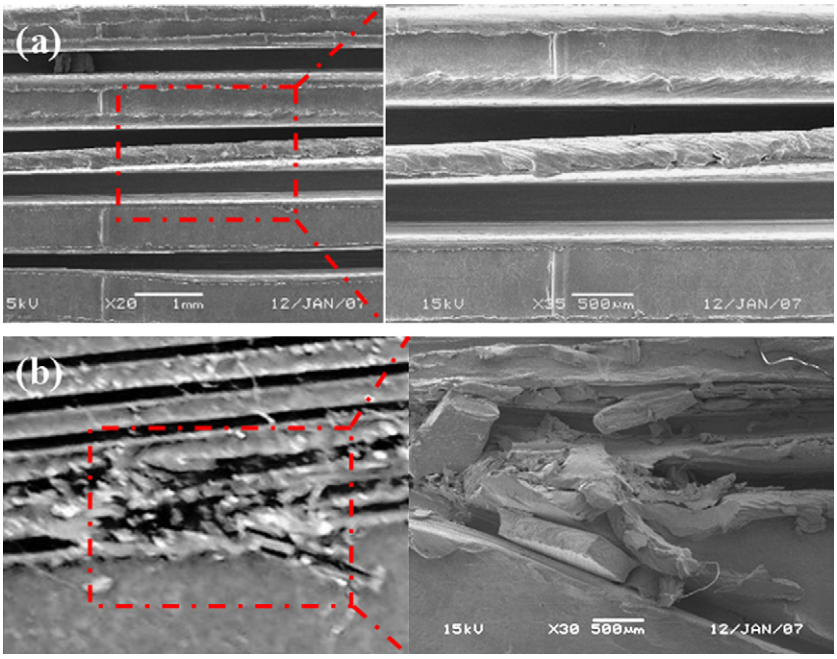


**Fig. 20.** Microchannel deformation due to tool gasket.

milling was almost the same as that of multi-cutter milling process; however, the work removal rate was much smaller than that of multi-cutter milling process.

Compared with the single-cutter milling process, multi-cutter milling process could dramatically reduce the machining time and improve the work removal rate due to simultaneous fabrication of multiple microchannels. Here, the machining time of five-cutter milling process was one-fifth lower than that of single-cutter milling process, but the work removal rate was five times larger. Obviously, the machining efficiency could be greatly improved by the lamination of much more cutters.

On the other hand, the microchannels fabricated by multi-cutter milling process had better pattern than that by reactive ion etching. As shown in Fig. 22, the bottom of microchannels fabricated by reactive ion etching was poorly defined due to the high pressure, and the sidewall angle is about 19° [33], whereas the multi-cutter milling process provided microchannels with a rectangular cross section.

### 4.4. Reaction characteristics of methanol steaming reforming

Fig. 23 presented the reaction characteristics of methanol steaming reforming under different GHSVs and reaction temperatures in the microchannel plate fabricated by multi-cutter milling process.

As shown in Fig. 23(a), methanol conversions under the same reaction temperature were decreased as the GHSV increased. As the GHSV increased, the contact time decreased leading to the decrease of methanol conversion. At the same GHSV, the methanol conversions increased as the reaction temperature increased due to the improvement of steam reforming reaction rate and the catalytic activity.

When the temperature was 450 °C, the methanol conversions over 90% would be achieved with a maximum GHSV restricted to 4000 ml $g^{-1}$ $h^{-1}$. With the larger GHSV at 450 °C, the methanol conversions maintained at least 65%. However, the methanol conversions were limited between 5% to 40% when reaction temperature was 400 °C and GHSV was larger than 15000 ml $g^{-1}$ $h^{-1}$. The reason was that only a microchannel plate was assembled inside the reformer during the experiments, excessive mixture of methanol and water directly flowed out the reformer without any reaction, leading to low methanol conversions. On the other hand, the GHSV and reaction temperature showed a litter effects on the hydrogen selectivity. The hydrogen selectivity on the plates could reach above 95%.

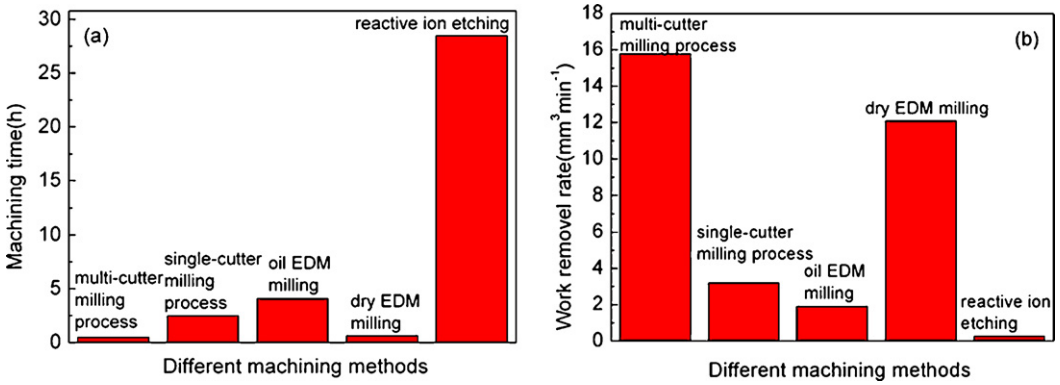


**Fig. 21.** Comparision of machining time and work removal rate.

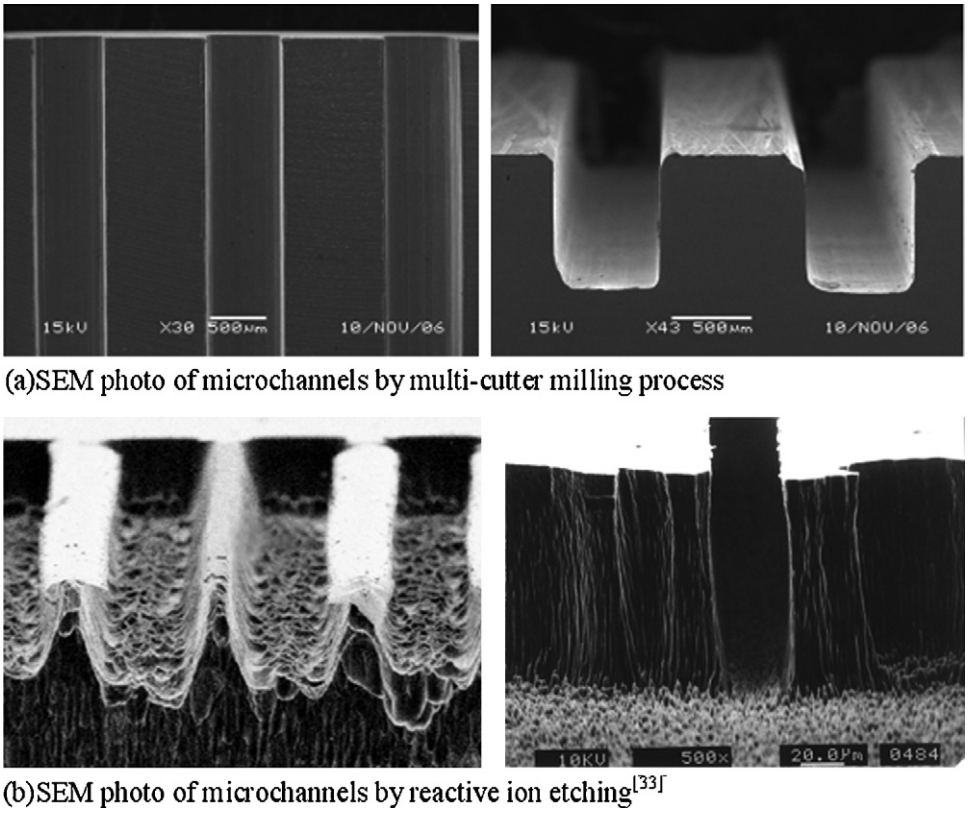


**Fig. 22.** Comparison of microchannel pattern. (a) SEM photo of microchannels by multi-cutter milling process. (b) SEM photo of microchannels by reactive ion etching [33].

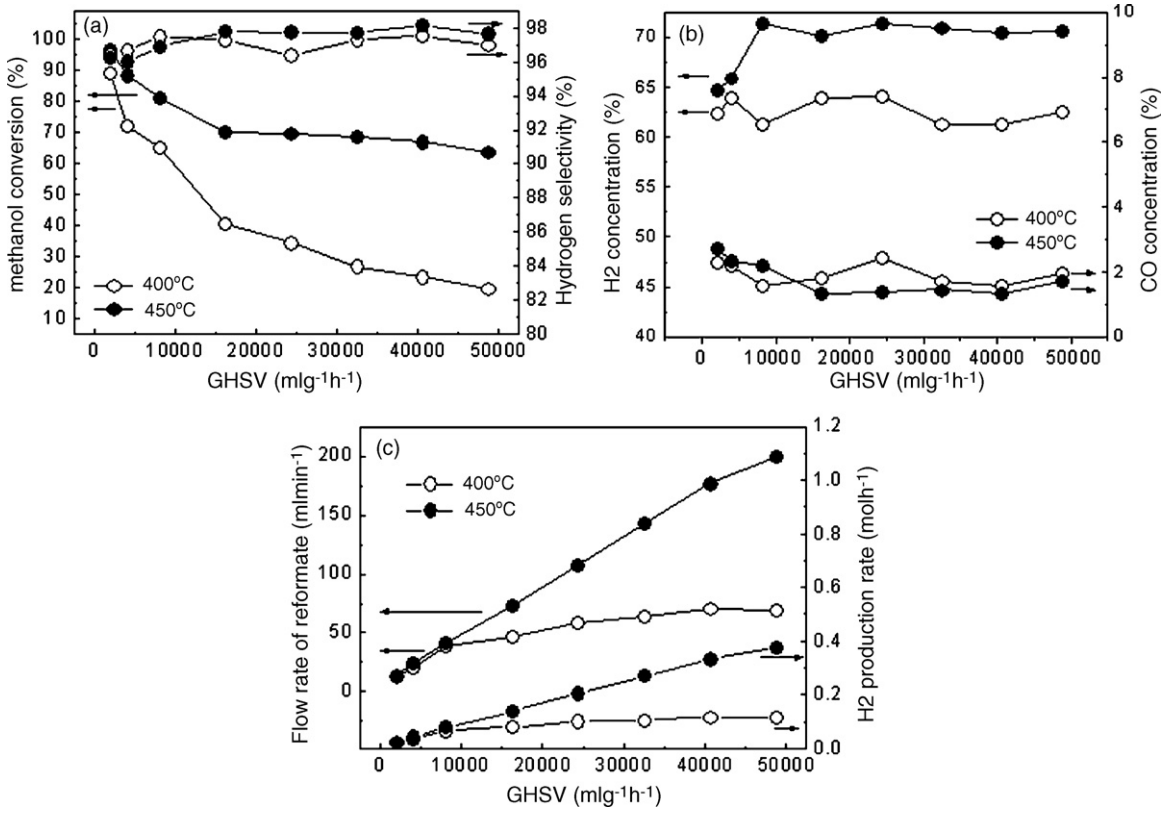


**Fig. 23.** Reaction characteristics of methanol streaming reforming.

As GHSV increased, the ratio of methanol steam in the reformate composite increased due to the decreased methanol conversions. As a result, the concentration of $H_2$ and CO slightly decreased with the increased GHSV. At the same GHSV, the $H_2$ concentration increased with the reaction temperatures due to the increased catalyst activity at higher temperature, as shown in Fig. 23(b). The $H_2$ concentrations almost kept in the range of 60–65%. However, when the reaction temperature reached to 450 °C, the $H_2$ concentration increased to nearly 73%. The CO concentrations varied between 1.4%∼2.9% under two reforming temperatures.

The flow rate of reformate and $H_2$ production increased with the increased GHSV at the same reaction temperature, as presented in Fig. 23(c). Under experimental conditions, the methanol reaction rate increased with GHSV while the hydrogen selectivity varied weakly, so the hydrogen production rate was increased with GHSV. As for the reaction temperature, higher temperature was favor for improving $H_2$ production rate due to the increased catalyst activity. The highest production rate was 0.38 mol $h^{-1}$, which was achieved at 450 °C with GHSV of 48757 ml $g^{-1}$ $h^{-1}$. The estimated electric power corresponded to about 12 W power output at the operating condition of 80% utilization ratio of $H_2$ and 60% efficiency of fuel cell.

## 5. Conclusions

A novel multi-cutter milling process for multiple parallel microchannels with manifolds is proposed to address the challenge of mass manufacture as required for cost-effective commercial application. The feasibility of new fabrication process was experimentally investigated under different machining conditions and the influences of cutting parameters and the composite tool on the microchannel qualities and burr formation were analyzed. Experimental results showed that larger cutting speed, smaller feed rate and cutting depth were in favor of obtaining relatively good microchannel qualities and small burrs.

According to the comparisons of experimental results of multi-cutter milling process and estimated one of other alternative methods, it found that multi-cutter milling process showed much shorter machining time and higher work removal rate than that of other alternative methods, including oil EDM milling, dry EDM milling and reactive ion etching. Compared with single-cutter milling process, one of the main advantages of multi-cutter milling process is the parallel processing of multiple microchannels at the same time, resulting in relatively cheap fabrication. In addition, high-aspect-ratio microchannels with manifolds on a large area sheet are easy to achieve. Reaction characteristics of methanol steam reforming in microchannels also indicated that multi-cutter milling process was probably suitable for a commercial application.

## Acknowledgments

This research was supported by the National Nature Science Foundation of China, Project No. 50805052, the Natural Science Foundation of Guangdong Province, Project No. 8451064101000320, the Doctoral Program of Ministry of Education of China, Project No. 200805611089, and Student Research Program of South China University of Technology.

## References

[1] A.V. Pattekar, M.V. Kothare, Journal of Microelectromechanical Systems 13 (1) (2004) 7–18.
[2] A.V. Pattekar, M.V. Kothare, A microreactor for in-situ hydrogen production by catalytic methanol reforming, in: Proceedings of the 5th International Conference on Microreaction Technology (IMRET 5), Strasbourg, France, 2001.
[3] K.S. Chang, S. Tanaka, C.L. Chang, M. Esashi, Comustor-intergrated micro-fuel processor with suspended membrane structure, in: The 12th International Conference on Solid State Sensors, Actuators and Microsystems, Boston, 2003, pp. 635–638.
[4] T. Kikas, H. Zhang, I. Bardenshteyn, C. Ejimofor, P. Puri, C. Philips, A.G. Fedorov, Feedstock for micro fuel cells: efficient hydrogen production in the reverse-flow autothermal catalytic microreactors, in: International Symposium on Micro/Nanoscale Energy Conversion, MECT-02, International Centre for Heat and Mass Transfer, Antalya, Turkey, 2002.
[5] B. Alm, U. Imke, R. Knitter, U. Schygulla, S. Zimmermann, Chemical Engineering Journal 135S (2008) S179–S184.
[6] P.M. Martin, D.W. Matson, W.D. Bennett, D.C. Stewart, Y. Lin, Laser micromachined and laminated microfluidic components for miniaturized thermal, chemical and biological systems, in: SPIE Conference Proceedings, Design, Test, and Micro-fabrication of MEMS and MOEMS, 3680, 1999, pp. 826–833.
[7] D.W. Matson, P.M. Martin, D.C. Stewart, A.L.Y. Tonkovich, M. White, J.L. Zilka, G.L. Roberts, Fabrication of microchannel chemical reactors using a metal lamination process, in: Proceedings of 3rd International Conference on Microreaction Technology (IMRET 3), Berlin, 2000, pp. 62–71.
[8] A. Tonkovich, D. Kuhlmann, A. Rogers, J. Mcdaniel, S. Fitzgerald, R. Arora, T. Yuschak, Chemical Engineering Research and Design 83 (A6) (2006) 634–639.
[9] P. Jiang, M. Fan, G. Si, Z. Ren, International Journal of Heat and Mass Transfer 44 (2001) 1039–1051.
[10] T. Henning, J.J. Brandner, K. Schubert, Chemical Engineering Journal 101 (2004) 339–345.
[11] G.G. Park, S.D. Yim, Y.G. Yoon, C.S. Kim, D.J. Seo, K. Eguchi, Catalysis Today 110 (2005) 108–113.
[12] G.G. Park, S.D. Yim, Y.G. Yoon, W.Y. Lee, C.S. Kim, D.J. Seo, K. Eguchi, Journal of Power Sources 145 (2005) 702–706.
[13] G. Chen, Q. Yuan, H. Li, Sh. Li, Chemical Engineering Journal 101 (2004) 101–106.
[14] E.R. Delsman, M.H.J.M. De Croon, A. Pierik, G.J. Kramera, P.D. Cobden, Ch. Hofmann, V. Cominos, J.C. Schoutena, Chemical Engineering Science 59 (2004) 4795–4802.
[15] A.L.Y. Tonkovich, J.L. Zilka, M.R. Powell, C.J. Call, The catalytic partial oxidation of methane in a micro-channel chemical reactor, in: 2nd International Conference on Microreaction Technology, Topical Conference preprints, New Orleans, USA, 1998, pp. 45–53.
[16] F. Marty, L. Rousseau, B. Saadany, B. Mercie, O. Français, Y. Mita, T. Bourouina, Microelectronics Journal 36 (2005) 673–677.
[17] D.P. Adams, M.J. Vasile, G. Benavides, A.N. Campbell, Journal of the International Societies for PrecisionEngineering and Nanotechnology. 25 (2001) 107–113.
[18] C.R. Friedrich, S.W. Kang, Precision Engineering 16 (1994) 56–59.
[19] H.D.M. Hettiarachchi, M. Golubovic, W.M. Worek, W.J. Minkowycz, International Journal of Heat and Mass Transfer (2008), doi:10.1016/j.ijheatmasstransfer.2008.02.049.
[20] S.K. Ryi, J.S. Park, S.H. Choi, S.H. Cho, S.H. Kim, Chemical Engineering Journal 113 (2005) 47–53.
[21] G.G. Park, D.J. Seo, S.H. Park, Y.G. Yoon, C.S. Kim, W.L. Yoon, Chemical Engineering Journal 101 (2004) 87–92.
[22] J.M. Sohn, Y.C. Byun, J.Y. Cho, J. Choe, K.H. Song, International Journal of Hydrogen Energy 32 (2007) 5103–5108.
[23] V. Cominos, V. Hessel, C. Hofmann, G. Kolb, R. Zapf, A. Ziogas, E.R. Delsman, J.C. Schouten, Catalysis Today 110 (2005) 140–153.
[24] A.L.Y. Tonkovich, J.L. Zilka, M.R. Powell, C.J. Call, The catalytic partial oxidation of methane in a micro-channel chemical reactor, in: 2nd International Conference on Microreaction Technology; Topical Conference preprints, New Orleans, USA, 1998, pp. 45–53.
[25] S. Filiz, C.M. Conley, M.B. Wasserman, O.B. Ozdoganlar, International Journal of Machine Tools & Manufacture (2007), doi:10.1016/j.ijmachtools.2006.09.024.
[26] Z. Yu, T. Jun, K. Masanori, Journal of Materials Processing Technology 149 (2004) 353–357.
[27] K. Lee, D.A. Dornfeld, Precision Engineering 29 (2005) 246–252.
[28] O. Olvera, G. Barrow, International Journal of Machine Tools & Manufacture 36 (9) (1996) 1005–1020.
[29] T. Lin, Journal of Materials Processing Technology 108 (2000) 12–20.
[30] C. Horny, L. Kiwi-Minsker, A. Renken, Chemical Engineering Journal 101 (2004) 3–9.
[31] X. Mu, L. Pan, N. Liu, C. Zhang, S. Li, G. Sun, S. Wang, International Journal of Hydrogen Energy 32 (2007) 3327–3334.
[32] H. Yu, H. Chen, M. Pan, Y. Tang, K. Zeng, F. Peng, H. Wang, Applied Catalysis A: General 327 (2007) 106–113.
[33] M. Kuhnke, Th. Lippert, E. Ortelli, G.G. Scherer, A. Wokaun, Thin Solid Films 453–454 (2004) 36–41.